



## Electro-assisted catalytic wet air oxidation of organic pollutants on a MnO@C/GF anode under room condition



Lin-Feng Zhai<sup>a</sup>, Ming-Feng Duan<sup>a</sup>, Meng-Xia Qiao<sup>a</sup>, Min Sun<sup>a,\*</sup>, Shaobin Wang<sup>b,\*</sup>

<sup>a</sup> Anhui Province Key Laboratory of Advanced Catalytic Materials and Reaction, School of Chemistry and Chemical Engineering, Hefei University of Technology, Hefei, 230009, China

<sup>b</sup> School of Chemical Engineering, The University of Adelaide, Adelaide, SA 5005, Australia

### ARTICLE INFO

**Keywords:**  
Wet air oxidation  
Manganese monoxide  
Electrocatalysis  
 $O_2$  activation  
Organic degradation

### ABSTRACT

Catalytic oxygen ( $O_2$ ) activation for oxidative removal of pollutants under ambient condition is important for pollution control. Herein, we report a hybrid of MnO catalyst confined in a porous carbon matrix on a graphite felt support (MnO@C/GF) for electro-activation of  $O_2$  toward degradation of various pollutants at ambient condition. The electro-assisted catalytic wet air oxidation (ECWAO) process on anodic MnO@C/GF is able to completely mineralize dyes and typical pharmaceuticals and personal care products. Mechanistic studies indicate the oxidation of the organic pollutants in the ECWAO process involves chemisorption of  $O_2$  on MnO, activation of the chemisorbed oxygen species via electro-oxidation reaction, and oxidation of organic pollutants by the activated chemisorbed oxygen species. The carbon matrix prevents MnO leaching during the ECWAO process, thus endowing the composite with excellent stability and reusability. The process demonstrates high efficiency, low energy input and environmental friendliness, exhibiting a great potential for practical wastewater treatment.

### 1. Introduction

Wet air oxidation (WAO) is a potent wastewater treatment technology that utilizes air to oxidize aqueous pollutants at elevated temperatures and pressures. The oxidation power of the system arises from dissolved molecular oxygen ( $O_2$ ) whose reactivity is dependent upon temperature. The reaction between  $O_2$  and organic pollutants is rather rapid at high temperatures, while it is hard to occur at room temperature because of the high activation energy which can exceed 200 kJ mol<sup>-1</sup> [1]. The rigid operation condition of WAO has stimulated the research for alternative  $O_2$  activation ways to overcome the thermal limitation of air oxidation.

An anodic electric field may be applied to activate  $O_2$  under ambient condition. Anodic oxidation processes have been used for degradation of various organic pollutants, and it is generally accepted that the pollutants are either directly electro-oxidized or oxidized by active oxygen species generated from water discharge [2]. However, Kapalka et al. has found the reaction of organic molecules and dissolved  $O_2$  can be induced in anodic oxidation process [3,4], but the underlying mechanism has not been fully elucidated yet. In light of the capability of  $O_2$  to oxidize organic molecules in an anodic electric field, we recently proposed an electro-assisted catalytic wet air oxidation (ECWAO)

process, which took advantage of anodic electric field to initiate air oxidation of rhodamine B on a graphite anode [5]. Later, it was reported that an organic pollutant phenol was more readily oxidized on a Fe<sub>3</sub>O<sub>4</sub>/graphite anode than on the graphite anode due to the catalysis of Fe<sub>3</sub>O<sub>4</sub>, but the reaction time was still too long as 51 h [6]. Since the electrode plays a catalytic role in such an ECWAO process, pollutant removal efficiency is anticipated to be improved by adopting an electrode with high catalytic activity towards  $O_2$  activation.

Manganese oxides (MnO<sub>x</sub>) are a group of important catalysts in air oxidation reactions owing to their remarkable capability to activate  $O_2$ . The adsorption of  $O_2$  molecules by manganese oxides is a typical chemisorption process involving the dissociation of  $O_2$  molecules on MnO<sub>x</sub> surface and formation of chemisorbed oxygen species. These adsorbed oxygen atoms are more reactive than pristine  $O_2$  molecules and serve as the main oxidants to various organic compounds [7]. Mn<sub>2</sub>O<sub>3</sub>, MnO<sub>2</sub> and Mn<sub>3</sub>O<sub>4</sub> in the manganese oxide family have been widespread used in oxidation reactions [8–10], while MnO is less studied because manganese tends to stay in a high oxidation state. However, it should be noted the unsaturated metal sites with a low valence state in a metal-containing catalyst usually present higher catalytic activities than their high-valence counterparts towards an oxidation reaction [11]. Notably, the unsaturated Mn<sup>II</sup> site in MnO has been identified as the key catalytic

\* Corresponding authors.

E-mail addresses: [sunmin81@mail.ustc.edu.cn](mailto:sunmin81@mail.ustc.edu.cn) (M. Sun), [shaobin.wang@adelaide.edu.au](mailto:shaobin.wang@adelaide.edu.au) (S. Wang).

center to undergo facile electron transfer as well as to provide active oxygen species for wet peroxide oxidation [12]. The superior catalytic behavior of MnO opens a way for improving the ECWAO performance by incorporating the MnO on a graphite anode.

In this work, we prepare a MnO catalyst confined in a porous carbon matrix on a graphite felt (GF) support ( $\text{MnO@C/GF}$ ). Such a  $\text{MnO@C/GF}$  composite shows a high and stable catalytic activity in the ECWAO reaction. A variety of biorefractory organic pollutants are degraded at high mineralization efficiencies on the  $\text{MnO@C/GF}$  anode by the ECWAO process performed under room condition. Mechanistic studies indicate the air oxidation of organic pollutants is initiated by the electro-activation of  $\text{O}_2$  on the MnO catalyst. The excellent catalytic activity of  $\text{MnO@C/GF}$  anode is attributed to the  $\text{Mn}^{II}$  site in MnO at which molecular  $\text{O}_2$  can effectively convert to highly active chemisorbed oxygen species.

## 2. Materials and methods

### 2.1. Synthesis and characterizations of $\text{MnO@C/GF}$ composite

Porous carbon embedded with MnO was synthesized on a GF support by one-pot co-assembly and high-temperature calcination, as illustrated in **Scheme 1**. In a typical synthesis, 0.5 g of manganese acetate and 0.1 g of polyacrylonitrile (PAN) were dissolved in 10 mL of *N,N*-dimethylformamide (DMF) to form a transparent solution. Next, a GF ( $2.5 \times 4 \text{ cm}^2$ , 3 mm in thickness) was immersed into the solution to adsorb manganese acetate and PAN. Then, the GF was taken out, dried at room temperature and heat-treated at 220 °C in air for 1 h to pre-oxidize the PAN and fix the manganese. Finally, the material was transferred into a tubular furnace and calcined at 900 °C in high-purity nitrogen ( $\text{N}_2$ ) atmosphere for 1 h to carbonize the PAN and produce MnO. For comparison, a C/GF composite was prepared in the absence of manganese acetate. In another synthesis, manganese acetate was loaded on a GF in the absence of PAN, and the final product was labelled as  $\text{MnO}_x/\text{GF}$  composite.

Valence states of manganese and oxygen species presented in  $\text{MnO@C/GF}$  composite were determined using X-ray photoelectron spectroscopy (XPS) on a Thermo ESCALAB 250 spectrometer (USA). Crystalline phase of manganese oxide was identified by X-ray diffractogram (XRD) using a Bruker D8 advance X-ray diffractometer (Germany). The content of manganese in the composite was determined by thermogravimetry (TG) on a Shimadzu TGA-50 apparatus (Japan) in air atmosphere. Morphology of the composite was observed on a Hitachi S-4800 scanning electron microscope (SEM, Japan) and a JEOL JEM-2100 F transmission electron microscope (TEM, Japan). Reducibility of  $\text{MnO@C/GF}$  composite was determined by hydrogen temperature-programmed reduction ( $\text{H}_2\text{-TPR}$ ) on a Quantachrome

ChemBET TPR/TPD apparatus (USA).

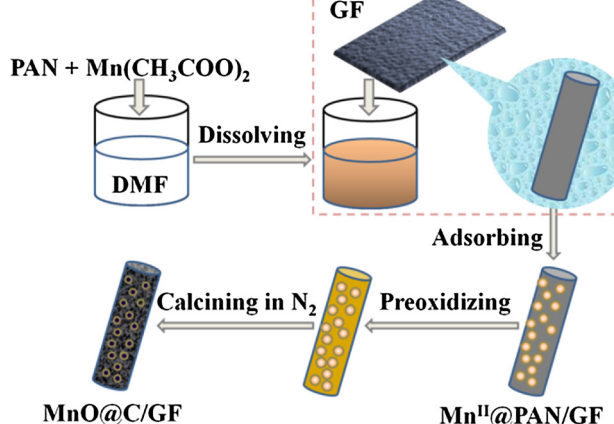
### 2.2. ECWAO for degradation of organic pollutants

The ECWAO system was operated in a 180-mL glass-made cylindrical reactor under room condition, using the prepared  $\text{MnO@C/GF}$  composite as the working electrode, a Pt wire ( $\Phi 0.5 \text{ mm} \times 37 \text{ mm}$ ) as the counter electrode and a saturated calomel electrode (SCE, +0.24 V vs. standard hydrogen electrode) as the reference. All electrode potential values reported are referred to SCE. A 120 mL of  $\text{Na}_2\text{SO}_4$  solution (50 mM, pH 7.0) was used as the electrolyte and fuchsin basic (FB, 50 mg L<sup>-1</sup>) was the model pollutant unless otherwise indicated. In some experiments, crystal violet, neutral red, tetracycline, bisphenol A and ibuprofen were subjected to degradation at a concentration of 50 mg L<sup>-1</sup>. The ECWAO process was initiated by imposing an anode potential of 0.8 V on the working electrode from a CHI 1000C electrochemical workstation (USA), and circuit current was recorded at 1-min interval. Air was bubbled at a rate of 1.5 L min<sup>-1</sup> from the bottom of the reactor to ensure the electrolyte was saturated with  $\text{O}_2$ . The concentration of dissolved  $\text{O}_2$  (DO) was measured using an AZ8403 DO meter (HengXin, China). The concentration of FB was monitored by measuring the absorbance at  $\lambda = 543 \text{ nm}$  on a 754 UV-vis spectrophotometer (JINHUA, China). Total organic carbon (TOC) was determined on a HTM-CT1000 M TOC analyzer (Tailin, China). Dissolved manganese was quantified by an inductively coupled plasma and optical emission spectrometer (ICP-OES) on an Agilent 700 apparatus (USA). The hydroxyl radical ( $\cdot\text{OH}$ ) was quantified with dimethyl sulfide (DMSO) trapping and liquid chromatography [13]. The reduction of nitro blue tetrazolium salt ( $\text{NBT}^{2+}$ ) was used to detect the superoxide anions [14], and an iodometric method was performed to determine the total amount of peroxodisulfate, hydrogen peroxide and ozone [15]. All experiments were conducted in triplicate, and the average values with standard deviations were presented.

Intermediate products generated from the degradation of FB were identified by gas chromatography-mass spectrometry (GC-MS). Solid-phase extraction was carried out to preconcentrate the products prior to GC-MS analysis. An Oasis HLB SPE cartridge (3 mL, 60 mg, Waters, USA) was conditioned with 5 mL of methanol and 5 mL of deionized water, and then 1000 mL of sample was loaded at a flow rate of approximately 10 mL min<sup>-1</sup>. Elution was performed with 5 mL of methanol, and the elute was subjected to GC-MS analysis on a Thermo Trace 1300 system equipped with a TR-V1 capillary column (30 m × 0.25 mm ID × 1.4 μm film, USA). High-purity helium was chosen as the carrier gas, and injection temperature was set at 280 °C. Column temperature was gradually increased from 100 to 250 °C at a rate of 10 °C min<sup>-1</sup>, and then to 280 °C at a rate of 30 °C min<sup>-1</sup>. Electron impact (EI) mass spectra were monitored from 50 to 500 m/z. The ion source and inlet line temperatures were set at 220 and 280 °C, respectively.

### 2.3. Cyclic voltammetry (CV)

The CV tests were conducted in a three-electrode cell-assembly with platinum counter electrode and SCE reference electrode. The working electrode was fabricated by loading the  $\text{MnO@C/GF}$  composite on a glassy carbon electrode (3 mm in diameter). Briefly, the  $\text{MnO@C/GF}$  composite was ground into powder of particle size less than 20 μm. Then, 6 mg of the powder was dispersed in 300 μL of anhydrous ethanol and 50 μL of Nafion solution (5 wt%) by ultrasonication. After that, 10 μL of resulting ink was dropped onto the glassy carbon electrode and dried at room temperature. The electrolyte was 50 mM  $\text{Na}_2\text{SO}_4$  solution (pH 7.0) which was pre-saturated with  $\text{N}_2$  or  $\text{O}_2$ . The concentration of FB in the electrolyte was 50 mg L<sup>-1</sup>. CV was carried out between -1.2 and 1.2 V at 0.1 V s<sup>-1</sup> on a CHI 660D electrochemical workstation (USA), with an initial scanning from low to high potential.



**Scheme 1.** Schematic illustration of the fabrication of  $\text{MnO@C/GF}$  composites.

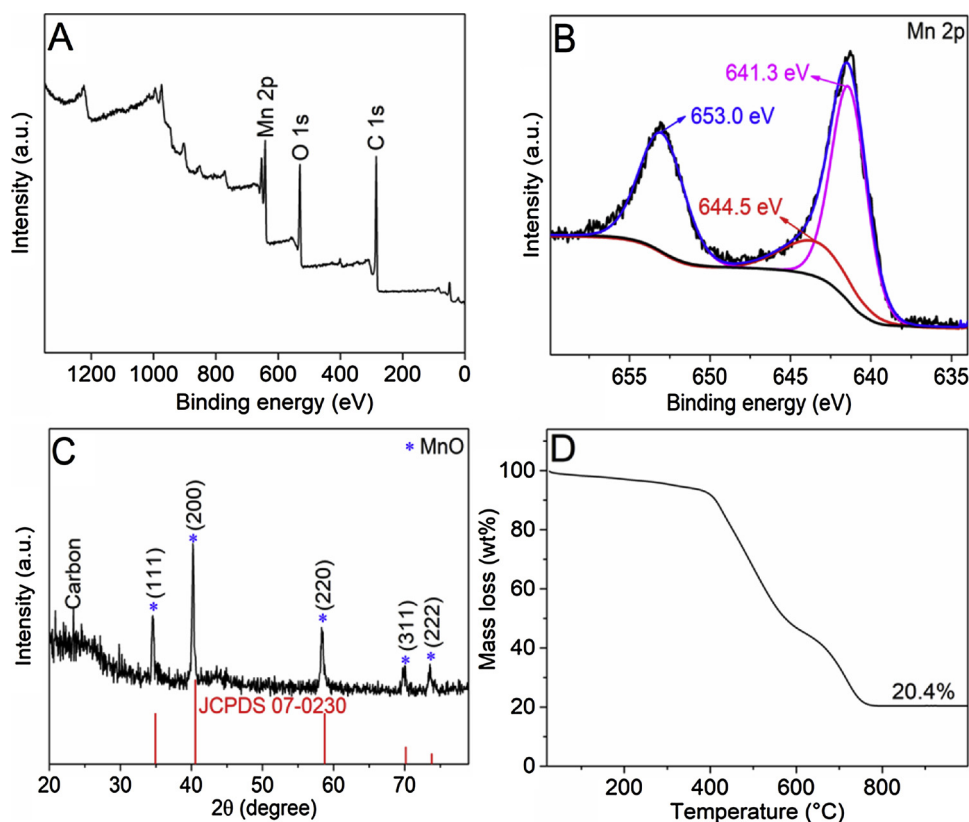


**Fig. 1.** XPS survey spectrum (A), high resolution Mn 2p XPS spectrum (B), XRD pattern (C) and TG curve (D) of the MnO@C/GF composite.

### 3. Results and discussion

#### 3.1. Structure and morphology of MnO@C/GF composite

Surface elemental analysis by XPS indicates the presence of carbon, oxygen and manganese in the MnO@C/GF composite (Fig. 1A). As shown in Fig. 1B, Mn 2p level is split into  $2p_{3/2}$  and  $2p_{1/2}$  doublets at 641.3 and 653.0 eV with  $2p_{3/2}$ - $2p_{1/2}$  spin-energy separation exactly being 11.7 eV, which is characteristic of Mn<sup>II</sup> valence state [16]. XRD pattern (Fig. 1C) of the MnO@C/GF composite shows a typical peak at  $2\theta$  value of 25° for GF support. Besides, other peaks at  $2\theta$  values of 34.9°, 40.5°, 58.7°, 70.2° and 73.8° are attributed to the (111), (200), (220), (311) and (222) planes of cubic MnO crystal (JCPDS, 07-0230). The manganese content in the composite is determined to be 14.7 wt% by TG analysis (Fig. 1D), in view that the final ash product after combustion in air is Mn<sub>3</sub>O<sub>4</sub> instead of MnO [12]. SEM images (Fig. 2A and B) show the surface of GF support is covered by a layer of porous carbon matrix from the carbonization of PAN, while MnO nanoparticles are embedded or encapsulated in the carbon matrix. The TEM image (Fig. 2C) demonstrates the sizes of MnO particles are ranged from 80 to 130 nm. Fig. 2D displays the high resolution TEM image with a clearly identified lattice fringe space of 2.23 Å, corresponding well to the (200) plane of cubic MnO.

#### 3.2. Pollutants degradation in the ECWAO process

Several biorefractory organic pollutants, including dyes, pharmaceuticals and personal care products, are subjected to degradation by the ECWAO process. As shown in Fig. 3A, crystal violet, neutral red, and FB are rapidly mineralized in 100 min, and tetracycline is mineralized by 75.1% in the same period of time. The process also shows favorable performance in degrading bisphenol A and ibuprofen. After 350 min, the TOC removal efficiency for bisphenol A is as high as 91.2% and it reaches 85.1% for ibuprofen. Therefore, the ECWAO process with

MnO@C/GF anode can be extensively used for deep mineralization of various biorefractory organic pollutants. Mineralization current efficiency (MCE) is used to evaluate the utilization efficiency of electrical charge by the ECWAO process in degrading organic pollutants. The MCE is expressed as the ratio of experimental TOC removal to theoretical TOC removal considering that the applied electrical charge is totally consumed to mineralize the organic pollutant, and is calculated as [17]:

$$MCE = \left[ \frac{nFV_s \Delta(TOC)_{exp}}{7.2 \times 10^5 m \int_0^t I dt} \right] \times 100\% \quad (1)$$

where  $n$  is the number of electrons involved in the combustion of carbon atoms in an organic pollutant,  $F$  is the Faraday constant (96,485 C mol<sup>-1</sup>),  $V_s$  is the solution volume (L),  $\Delta(TOC)_{exp}$  is the experimental TOC decay (mg L<sup>-1</sup>),  $7.2 \times 10^5$  is the conversion factor (60 s min<sup>-1</sup> × 12,000 mg-carbon mol<sup>-1</sup>),  $m$  is the number of carbon atoms in the organic pollutant and  $I$  is the circuit current (A) at electrolysis time  $t$  (min). Generally speaking, the MCEs of conventional anodic oxidation systems are significantly lower than 100% due to inevitable charge loss in the anodic reaction [17–19]. In contrast, the MCEs of the current ECWAO process in treating the different pollutants are all higher than 170% owing to the considerable contribution of catalytically activated O<sub>2</sub> to the mineralization of pollutants (Fig. 3B). Notably, the MCE values of even higher than 200% suggests the pollutants are mineralized via catalytic air oxidation rather than anodic oxidation.

Next, FB is selected as a probe pollutant and its adsorption and degradation on the MnO@C/GF electrode is investigated. The reactor is continuously bubbled with N<sub>2</sub> gas overnight to allow adsorption equilibrium of FB. As shown in Fig. 3C, the MnO@C/GF electrode demonstrates a limited adsorption capacity of FB with only 15.2% of TOC removal. Upon initiation of ECWAO, the TOC is rapid depleted within 80 min. In comparison, the TOC removal efficiency is only 26.9% on C/GF electrode, indicating the important role of MnO in catalyzing the

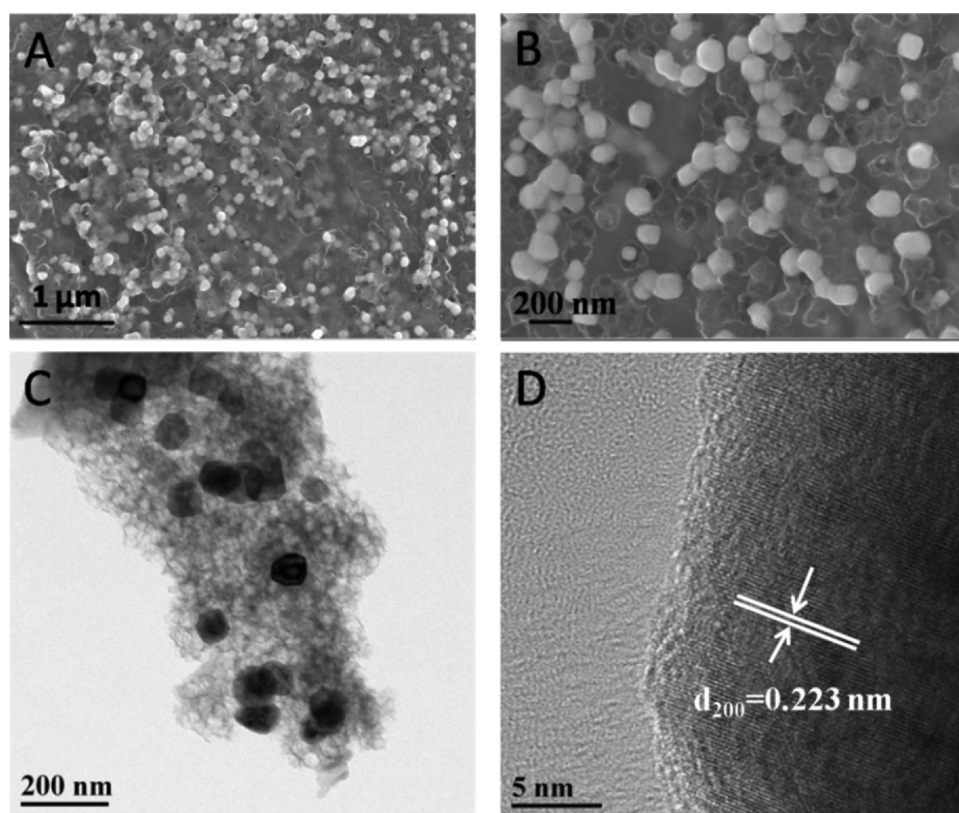


**Fig. 2.** SEM (A and B) and TEM images (C and D) of the MnO@C/GF composite.

ECWAO. The TOC is removed by 63.4% on  $\text{MnO}_x/\text{GF}$  electrode. Structure characterization indicates the presence of  $\text{Mn}_3\text{O}_4$  in such a material, and manganese content is only 9.1 wt% as determined by TG analysis (Fig. 4). Such results suggest the importance of carbon matrix in MnO@C/GF composite, which not only protects MnO from oxidation during the fabrication process but also spatially confine the MnO to ensure high manganese loading on the GF support. The indirect anodic oxidation process with boron-doped diamond (BDD,  $2.5 \times 4 \text{ cm}^2$ , diamond layer of  $10 \mu\text{m}$ , CSEM, Switzerland) electrode is also operated at 0.8 V for performance comparison. As shown in Fig. 3C, FB is hardly mineralized via indirect anodic oxidation at such a low electrode potential. As a matter of fact, FB is a typical triphenylmethane compound which usually shows partial mineralization behavior in chemical or physicochemical degradation processes [20–22]. The rapid and complete mineralization of FB in the ECWAO process reflects the effectiveness of the process for oxidation. What should be noted is that FB fails to be degraded by air in the absence of an electric field, and is mineralized at only 34.8% after adsorption on MnO@C/GF electrode without air participation, implying both  $\text{O}_2$  and electric field are indispensable for effective degradation of FB. Fig. 3D and E show that the ECWAO process is able to maintain stable efficiency to degrade FB in eight successive fed-batch cycles under neutral conditions, suggesting excellent reusability of the MnO@C/GF electrode. The manganese content in the electrode underwent two cycles at pH 7.0 is 13.8 wt%, which is a bit lower than that in the fresh one (14.7 wt%), and no metal loss is detected in subsequent six cycles. In addition, the concentration of dissolved manganese in the solution after eight cycles is below the detection limit of ICP. The slight metal loss and negligible metal leaching can be attributed to the excellent confinement of MnO by porous carbon matrix. Such a superior stability of MnO@C/GF electrode also enables it to be readily used in acidic and alkaline solutions. Furthermore, the ECWAO process operated at pH 10.0 can well mineralize FB in eight cycles (Fig. 3E). For the process operated at pH 3.0, mineralization profiles of FB in the first five cycles are similar to that

obtained at pH 7.0 and 10.0. The time required for the total mineralization of FB is prolonged from 100 to 130 min in the next three cycles. Notably, the confined MnO in MnO@C/GF electrode displays favorable stability in acid solution. Metal content in the MnO@C/GF electrode is lost by only 7.4% after the eight cycles, and the concentration of manganese dissolved in acid solution is merely  $6.5 \text{ mg L}^{-1}$ .

Intermediate products generated from FB degradation are identified by GC–MS. As shown in Fig. 5A, the peaks at the retention time of 2.27, 4.19, 5.40, 14.59 and 15.47 min in the GC chromatograms of degraded samples are assigned to intermediate products. MS spectral analysis identifies them as phenol ( $m/z = 94$ ), m-cresol ( $m/z = 108$ ), methylhydroquinone ( $m/z = 124$ ), mono-hydroxybenzophenone ( $m/z = 198$ ) and diaminobenzophenone ( $m/z = 212$ ), respectively. Peak intensity of phenol on GC chromatogram gradually increases along with the degradation time until it achieves the highest at 60 min, and then visibly weakened at 80 min. In comparison, peak intensities of the other intermediate products reach the highest after 20 min of degradation, and then decrease until they disappear from the GC chromatogram at 80 min. Based on the evolution profiles of these intermediate products, we propose a possible route of FB degradation in the ECWAO process (Scheme 2). FB is firstly cleaved at the C=C side chain bond producing 4-amino-m-cresol and 4,4'-diaminobenzophenone as products. The 4-amino-m-cresol is subsequently converted to m-cresol via deamination, and then undergoes OH-substitution yielding 4-methylhydroquinone, 3-methylhydroquinone or 2-methylhydroquinone [23]. Meanwhile, the diaminobenzophenone is converted to mono-hydroxybenzophenone through sequential deamination and OH-substitution, followed by cleavage at the C=O bond between the two aromatic rings to yield phenol as the product [24]. Further oxidation of methylhydroquinone and phenol results in various carboxylic acids, such as fumaric acid, maleic acid and oxalic acid, as occurring in wet air oxidation or electrochemical oxidation systems [25,26]. Finally, these carboxylic acids are oxidized into carbon dioxide and water.

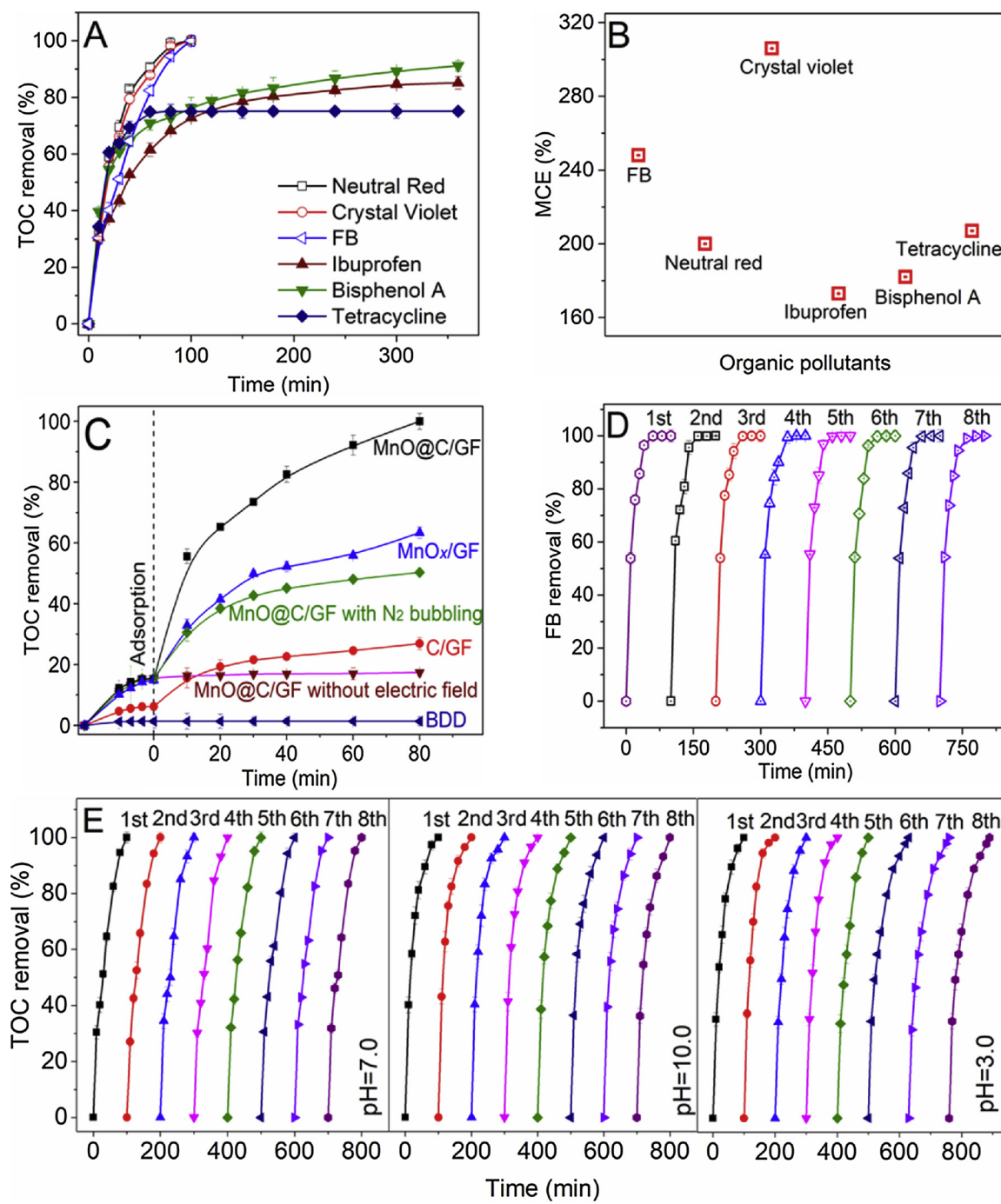


**Fig. 3.** Mineralization efficiencies of different organic pollutants in the ECWAO process (A) and corresponding MCEs (B); Mineralization efficiencies of FB on different anodes (C); Removal efficiency of FB in eight successive fed-batch cycles of ECWAO process (D); and mineralization efficiencies of FB in eight cycles of ECWAO process operated at different pHs (E). Electrode potential is at 0.8 V and solution pH in (A)-(D) is at 7.0.

### 3.3. Active oxygen species responsible for oxidation of pollutants in the ECWAO process

Previous studies indicated that O<sub>2</sub> was able to react with free organic radicals arising from the reaction between organic compound and ·OH [3]. In this ECWAO process, ·OH is indeed generated. However, its concentration is quite low at  $28.2 \times 10^{-6}$  mol L<sup>-1</sup> due to the low electrode potential at 0.8 V (Fig. 6A). Notably, the concentration of ·OH generated on the MnO@C/GF electrode is similar to that on the C/GF electrode, implying the more effective degradation of pollutants on MnO@C/GF electrode is not attributed to ·OH. Further, radical quenching experiments are conducted with tertiary butanol (t-BuOH)

and DMSO as radical scavengers of ·OH. The hydrophilic t-BuOH mainly quenches dissolved ·OH in solution and hydrophobic DMSO is able to quench adsorbed ·OH on the electrode surface. The concentration of scavengers is 1000 times greater than that of FB to ensure ·OH is totally quenched. As shown in Fig. 6B, the removal of FB, although being slowed down, is still accomplished on the MnO@C/GF electrode in the presence of t-BuOH/DMSO, suggesting the ECWAO process can be initiated without ·OH. Moreover, the generation of other reactive oxygen species, including superoxide radical, peroxodisulfate, hydrogen peroxide and ozone, is ignorable in the ECWAO process. Thus, they do not make contributions to FB degradation in the ECWAO process either.

CV is applied to characterize the electron transfer among FB, O<sub>2</sub> and

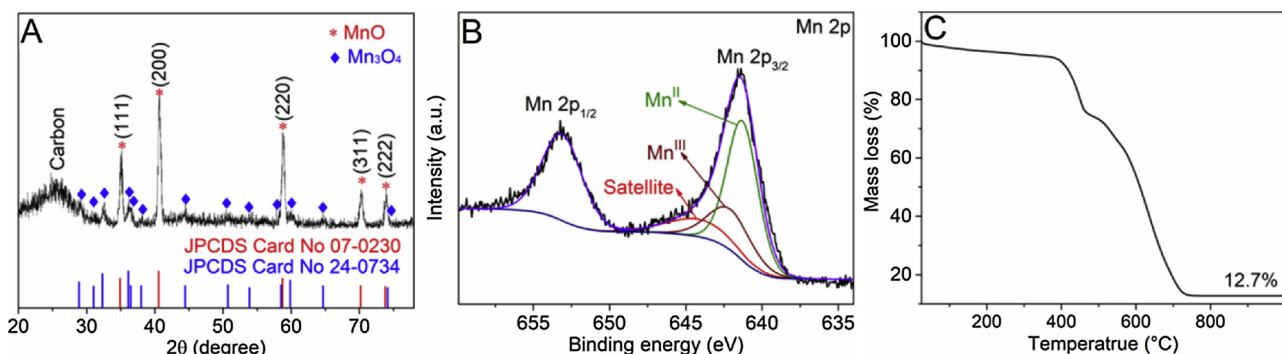


Fig. 4. XRD pattern (A), high resolution Mn 2p XPS spectrum (B) and TG curve (C) of the MnO<sub>x</sub>/GF composite.

the MnO@C/GF electrode in the electric field. As shown in Fig. 6C, the cyclic voltammogram of MnO@C/GF electrode in deoxygenated Na<sub>2</sub>SO<sub>4</sub> electrolyte features one large anodic peak centered at 0.79 V (Peak 1). Such a peak is attributed to the oxidation of Mn<sup>II</sup> to Mn<sup>III/IV</sup> [27], and it is not observed in the voltammogram of C/GF composite. Correspondingly, the reduction of Mn<sup>IV</sup> via Mn<sup>III</sup> to Mn<sup>II</sup> is reflected by

two cathodic peaks at 0.77 and 0.22 V, respectively (Peaks 3 and 4). The peaks attributed to Mn<sup>III</sup> and Mn<sup>IV</sup> reductions are also found in the voltammogram of MnO@C/GF electrode in deoxygenated FB solution, which means that the generated Mn<sup>III/IV</sup> species do not react with FB. Besides the anodic peak of Mn<sup>II</sup> oxidation, another small anodic peak is observed to start at 0.15 V (Peak 2) in the voltammogram of MnO@C/

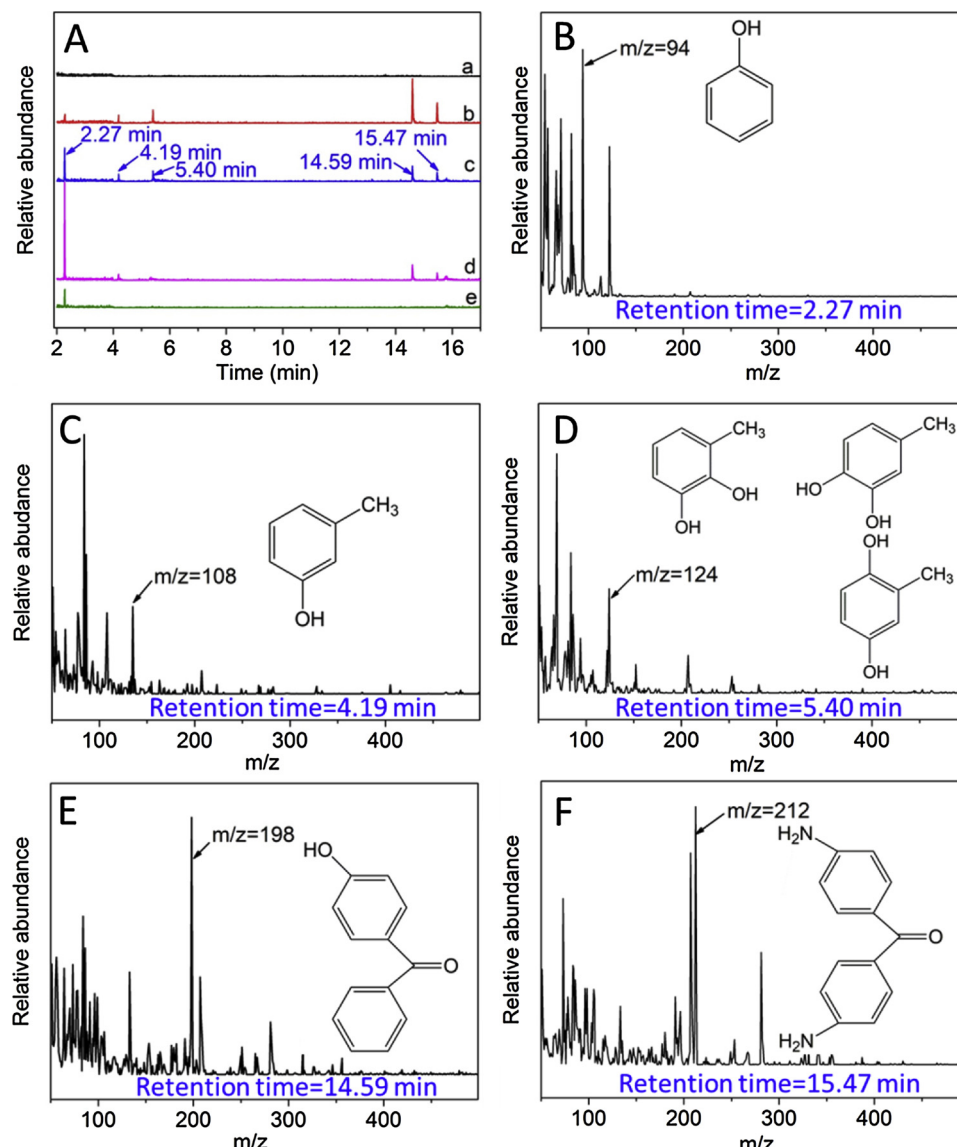
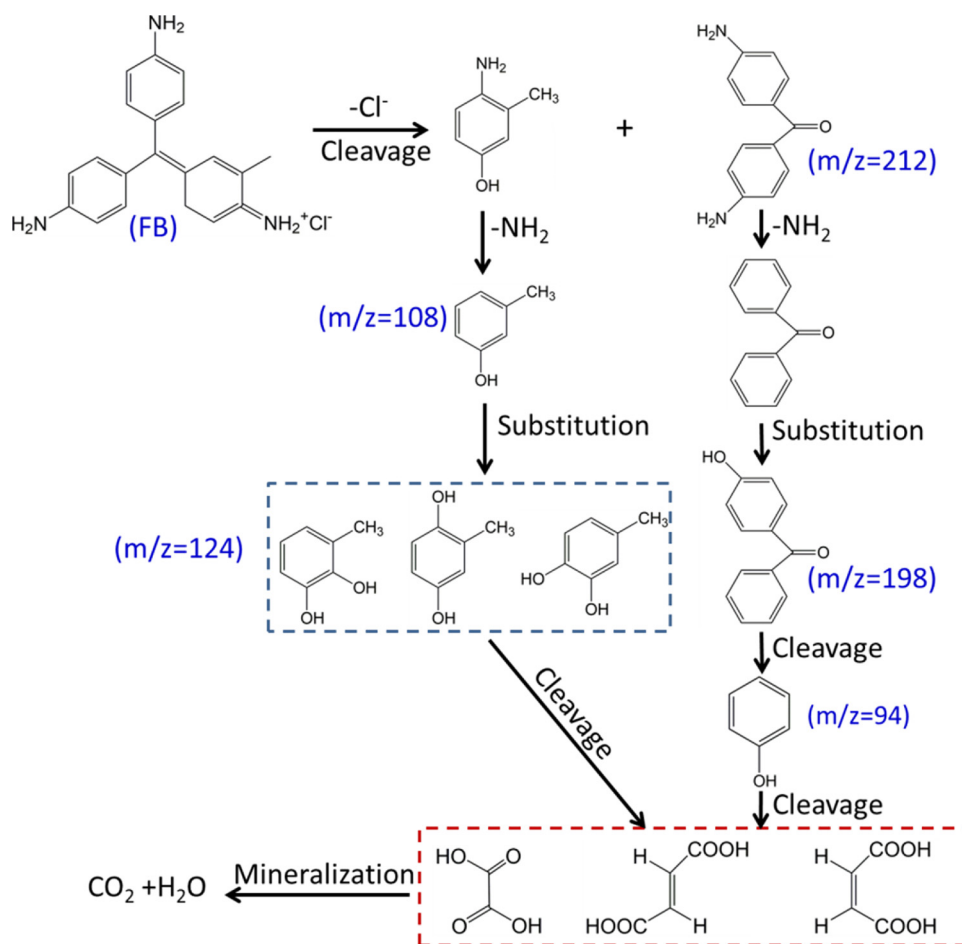


Fig. 5. GC chromatograms of intermediate products generated from FB degradation at different degradation times (A), and their corresponding mass chromatograms (B, C, D, E and F). The GC chromatograms a, b, c, d and e in Fig. 5A are referred to the samples obtained at degradation time of 0, 20, 40, 60 and 80 min, respectively.



Scheme 2. Proposed degradation pathway of FB in the ECWAO process.

GF electrode in deoxygenated Na<sub>2</sub>SO<sub>4</sub> electrolyte, and its corresponding cathodic peak is at -0.14 V (Peak 5). Noticing such the two peaks are not observed in the voltammogram of C/GF electrode, they represent another couple of redox reactions occurring on MnO. When the CV is conducted in deoxygenated FB solution, Peak 2 is still observable but Peak 5 disappears, suggesting the species generated via the reaction represented by Peak 2 can be consumed by FB. Notably, Fig. 6C shows Peak 2 is remarkably strengthened when O<sub>2</sub> is amended in solution, and its intensity is positively dependent upon the concentration of dissolved oxygen (DO). Obviously, the intensification of Peak 2 by O<sub>2</sub> is a result of the combination between MnO and O<sub>2</sub>.

In order to elucidate the manner of O<sub>2</sub> bonding to MnO, O1s XPS spectrum is used to identify the oxygen species in the MnO@C/GF composite (Fig. 7A). By comparing the O 1s levels for the C/GF and MnO@C/GF composites, three types of oxygen species are identified for MnO. The peak at binding energy of 529.4~530.1 eV belongs to the lattice oxygen (O<sub>2</sub><sup>2-</sup>) in MnO crystallites (O<sub>lat</sub>), and the one at binding energy of 531.2~531.8 eV is assigned to the chemisorbed oxygen species (O<sub>ads-c</sub>) such as O<sup>-</sup> and O<sub>2</sub><sup>-</sup> [28]. Finally, the peak at binding energy of 532.0~533.0 eV is associated with physically adsorbed oxygen species (O<sub>ads-p</sub>), which can be molecular water or physically adsorbed O<sub>2</sub> [29]. The H<sub>2</sub>-TPR profile of the MnO@C/GF composite gives two peaks at 350 and 550 °C, which are assigned to oxidations of H<sub>2</sub> by surface adsorbed and lattice oxygen species in MnO, respectively (Fig. 7B). In comparison, C/GF composite shows poor oxidation power as no obvious H<sub>2</sub> oxidation peak is observed in its H<sub>2</sub>-TPR profile. Transition metal oxides possess active surface for adsorbing O<sub>2</sub>, and the Mn<sup>II</sup> in MnO is apt to donate electrons to the adsorbed O<sub>2</sub> to form electron-rich O<sub>2</sub><sup>-</sup> and O<sup>-</sup> [30]. The highly active O<sup>-</sup>/O<sub>2</sub><sup>-</sup> species are

commonly the main oxidizers of organic compounds in air oxidation occurring at high temperatures [8,31]. In this view, the electro-oxidation reaction represented by Peak 2 (Fig. 6C) is proposed to be the activation of O<sup>-</sup>/O<sub>2</sub><sup>-</sup> species for oxidation reaction at room temperature. Such a proposition is confirmed by the different degradation behaviors of FB at 0.15 and 0.50 V (Fig. 6D). FB is not degraded at 0.15 V because of the low electrode potential unable to activate O<sub>2</sub>, while obvious degradation is observed at 0.50 V which is high enough to activate the O<sub>2</sub>. Fig. 6D also shows the degradation of FB in the reactor with saturated O<sub>2</sub> but sealed from ambient atmosphere. The consumption of O<sub>2</sub> is evidenced by the gradually decreased concentration of DO, and the degradation rate of FB in the reactor is lower than that in continuous air bubbling reactor due to the shortage of O<sub>2</sub>.

As mentioned above, O<sub>2</sub> activation on MnO surface is coupled with oxidation of MnO. Actually, crystalline MnO is partially transformed to amorphous Mn<sup>III</sup> species during the ECWAO process, as evidenced by the emergence of Mn 2p<sub>3/2</sub> peak at 641.8 eV, characteristic of Mn<sup>III</sup>, on the Mn 2p XPS spectrum of the composite underwent eight cycles of ECWAO (Fig. 7C) [32]. Meanwhile, the diffraction peaks of MnO in XRD pattern of the used composite are obviously weakened as compared to the fresh MnO (Fig. 7D), implying a decrement of crystal MnO in composite due to its partial oxidation. However, new MnO<sub>x</sub> phase other than MnO does not appear in the XRD pattern, suggesting the crystal MnO is partially transformed to amorphous Mn<sup>III</sup> species. Such a transformation creates more surface defects in MnO and favors the adsorption of O<sub>2</sub>, as evidenced by the increased peak area percentage of adsorbed oxygen species on O1s XPS spectrum of the used MnO@C/GF composite (Fig. 7A). In fact, Mn<sup>III</sup> species with labile Mn-O bonds have been found to be more catalytically active than Mn<sup>II</sup> species for

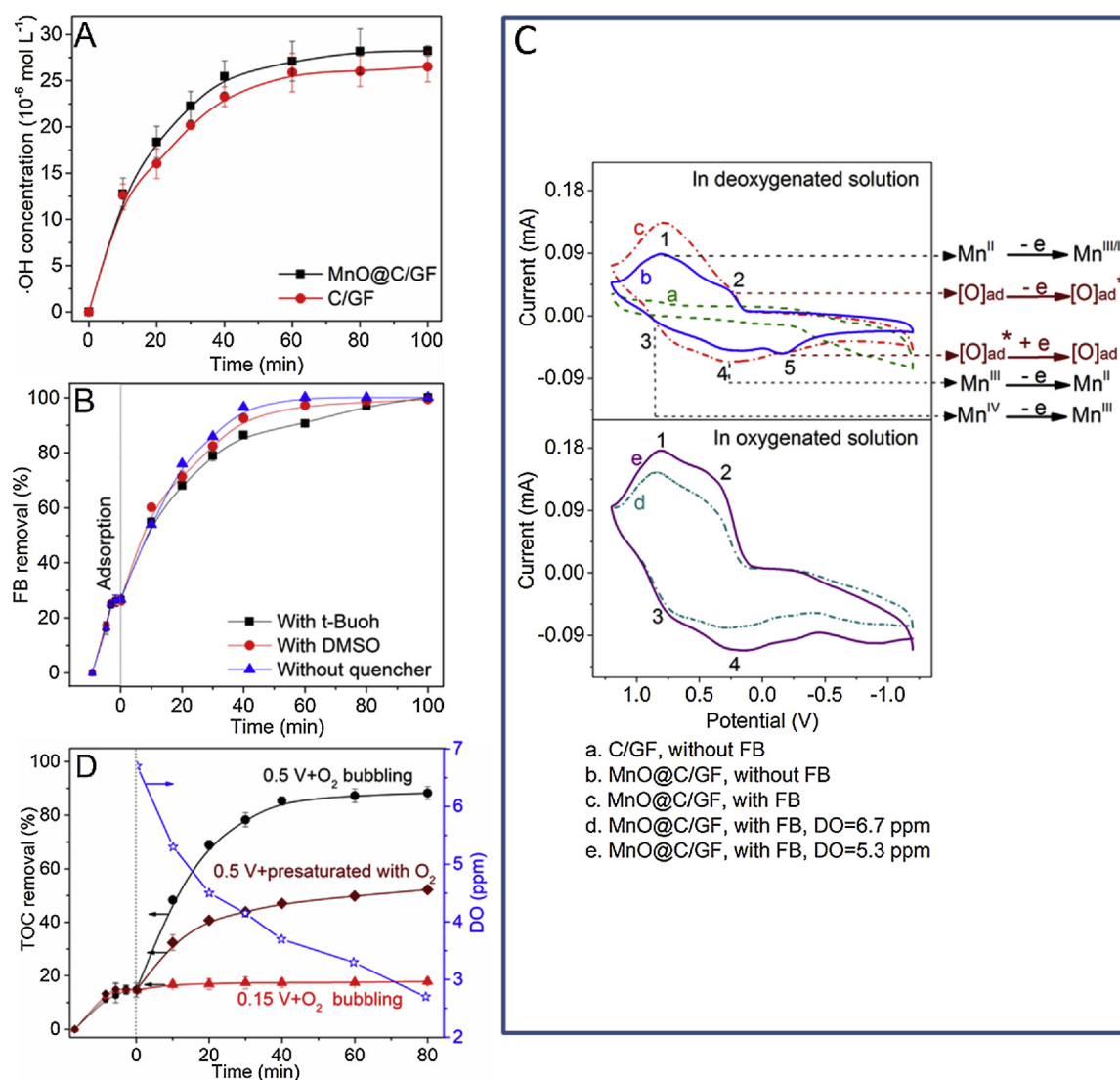


**Fig. 6.** Concentration of ·OH generated on the MnO@C/GF and C/GF electrodes during ECWAO process. (A); removal efficiencies of FB on the MnO@C/GF electrode in the presence of different ·OH quenchers (B); CV curves of the MnO@C/GF and C/GF electrodes under different conditions (C); and mineralization efficiencies of FB on the MnO@C/GF electrode at different anode potentials (D). Solution pH is at 7.0, and electrode potential in (A) and (B) is at 0.8 V.

oxidation [33], and the Mn<sup>III</sup> itself possesses ability for the selective partial oxidation of organic substances [34]. Therefore, the MnO@C/GF composite benefits from the transformation of crystal MnO to amorphous Mn<sup>III</sup> species as it provides more active sites for the reaction between pollutants and O<sub>2</sub>.

Based on above analysis, a diagram for the oxidation of organic pollutants by O<sub>2</sub> on anodic MnO@C/GF is proposed in Fig. 8. O<sub>2</sub> is firstly adsorbed onto MnO, and then transformed to chemisorbed O<sup>-</sup>/O<sub>2</sub><sup>-</sup> species accompanied by the shift of electron density from Mn<sup>II</sup> to the adsorption center. Next, the O<sup>-</sup>/O<sub>2</sub><sup>-</sup> species convert to their activated states via electro-oxidation in the electric field, and the Mn<sup>II</sup> at the adsorption centers is partially oxidized to Mn<sup>III</sup>. Finally, organic pollutant is oxidized by the activated O<sup>-</sup>/O<sub>2</sub><sup>-</sup> species on MnO surface. These steps are dependent upon the availability of the active sites in MnO for O<sub>2</sub> adsorption, and mediated by the redox reactions of Mn<sup>II</sup>/Mn<sup>III</sup> species [35].

#### 3.4. Significance of this work

Air oxidation technology is eco-friendly as compared to other advanced oxidation technologies using harmful and expensive oxidizing agents like ozone and hydrogen peroxide. However, conventional air

oxidation processes have to be performed at elevated temperatures due to the low oxidization power of molecular O<sub>2</sub> at room temperature. Taking the WAO as an example, organic pollutants are usually oxidized in the liquid phase at temperatures above 100 °C [36]. Even the so-called low temperature catalytic oxidation of volatile organic compounds still requires the operation at higher-than-room temperature [37]. In this work, we have demonstrated effective degradation of a variety of biorefractory organic pollutants by the ECWAO process under room condition. It opens an opportunity for developing more cost-effective WAO processes for practical wastewater treatment.

The ECWAO process also offers economic advantages as compared to conventional anodic oxidation processes, which generally achieve satisfactory removal of pollutants by adopting high voltages or currents. For example, the widely used indirect anodic oxidation needs high operational potential for water discharge in order to produce sufficient free radicals to oxidize pollutants [38]. In contrast, the electrode potential of the ECWAO process (0.8 V) is significantly lower than that used in most anodic oxidation processes for energy saving. Attributed to the high catalytic activity of MnO to air oxidation, the ECWAO process with MnO@C/GF anode enables rapid and deep oxidation of pollutants at low energy consumption.

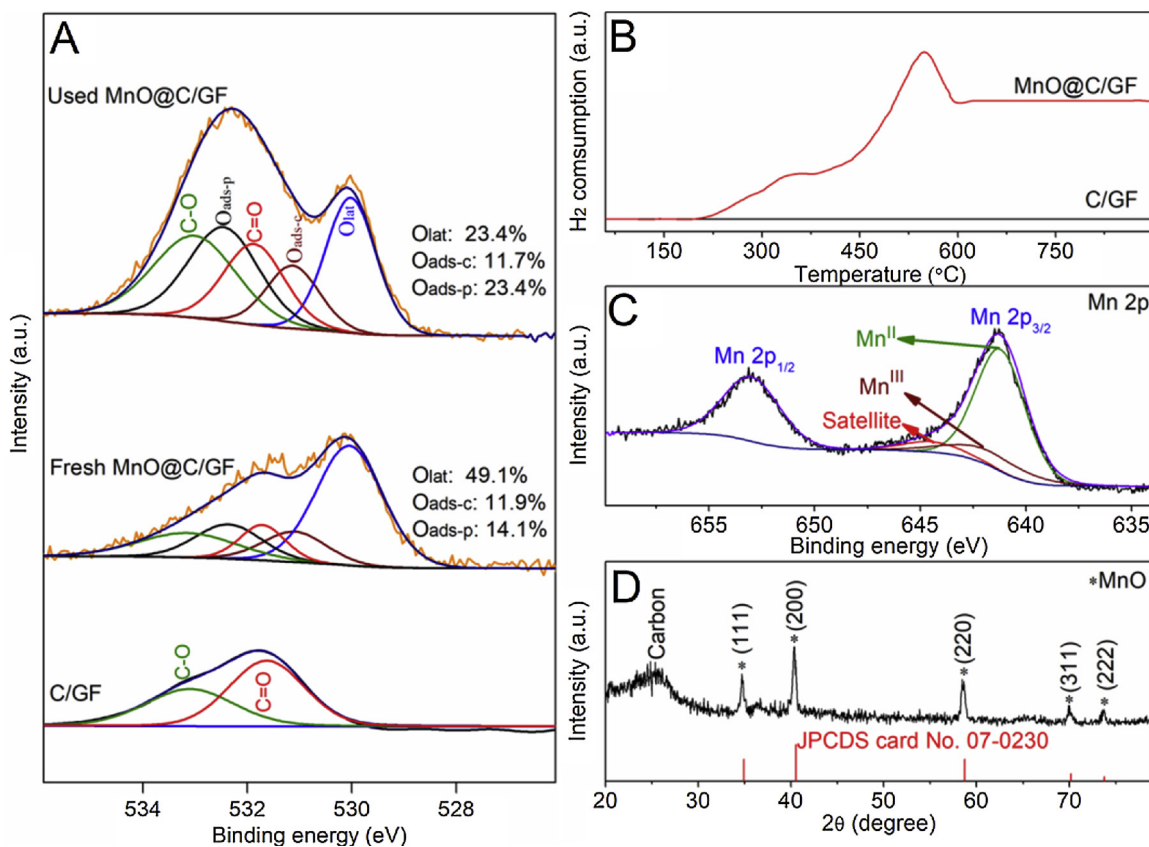


**Fig. 7.** High resolution O1s XPS spectra of the C/GF, fresh and used MnO@C/GF composites (A); H<sub>2</sub>-TPR profiles of the C/GF and MnO@C/GF composites (B); Mn 2p XPS spectrum (C) and XRD pattern (D) of the used MnO@C/GF composite.

#### 4. Conclusions

The ECWAO process on MnO@C/GF electrode is able to degrade a variety of biorefractory organic pollutants with high mineralization efficiencies. Such a process produces MCE values generally higher than 170% in the degradation of various organic pollutants, suggesting the pollutants are mineralized mainly via catalytic air oxidation reaction rather than anodic oxidation reaction. The MnO in the MnO@C/GF composite shows a high activity to catalyze air oxidation in anodic

electric field, and its confinement by porous carbon matrix endows the composite with favorable stability and reusability. The oxidation of pollutants by air in the ECWAO process is initiated by the electro-activation of O<sub>2</sub> on MnO, which involves dissociative adsorption of O<sub>2</sub> on the MnO and electron-oxidation of surface oxygen species in anodic electric field. The ECWAO process demonstrates the advantages of environmental friendliness and cost effectiveness for the treatment of wastewaters under room condition.

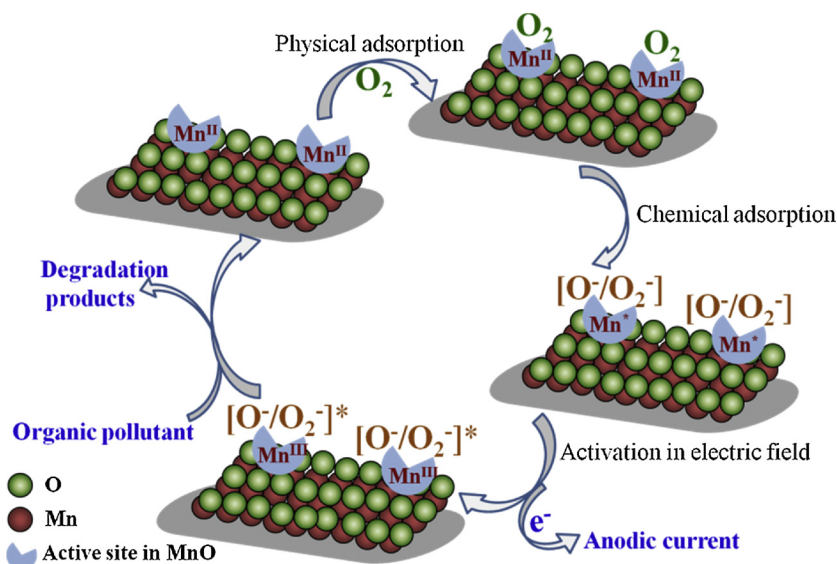


**Fig. 8.** Proposed catalytic oxidation pathway of pollutants by O<sub>2</sub> in the ECWAO process.

## Acknowledgements

The authors wish to thank the National Natural Science Foundation of China (51478157, 51378166) and the Program for New Century Excellent Talents in University (NCET-13-0767) for financial support of this work.

## References

- [1] H. Debellefontaine, J.N. Foussard, Wet air oxidation for the treatment of industrial wastes: chemical aspects, reactor design and industrial applications in Europe, *Waste Manage.* 20 (2000) 15–25.
- [2] C.A. Martinez-Huitle, M.A. Rodrigo, I. Sires, O. Scialdone, Single and coupled electrochemical processes and reactors for the abatement of organic water pollutants: a critical review, *Chem. Rev.* 115 (2015) 13362–13407.
- [3] A. Kapalka, B. Lanova, H. Baltruschat, G. Fóti, C. Comninellis, Electrochemically induced mineralization of organics by molecular oxygen on boron-doped diamond electrode, *Electrochim. Commun.* 10 (2008) 1215–1218.
- [4] G.R. de Oliveira, C.K.C. de Araujo, C.A. Martinez-Huitle, D.R. da Silva, Complementary mechanism model for the electrochemical mineralization, *Curr. Org. Chem.* 16 (2012) 1957–1959.
- [5] M. Sun, Y. Liu, W. Xiang, L.F. Zhai, Electricity-induced catalytic oxidation of RhB by O<sub>2</sub> at a graphite anode, *Electrochim. Acta* 158 (2015) 314–320.
- [6] L. Lei, L.M. Fang, L.F. Zhai, R. Wang, M. Sun, Anodic oxidation-assisted O<sub>2</sub> oxidation of phenol catalyzed by Fe<sub>3</sub>O<sub>4</sub> at low voltage, *Electrochim. Acta* 261 (2018) 394–401.
- [7] J. Yang, J.J. Xu, Nanoporous amorphous manganese oxide as electrocatalyst for oxygen reduction in alkaline solutions, *Electrochim. Commun.* 5 (2003) 306–311.
- [8] M. Piumetti, D. Fino, N. Russo, Mesoporous manganese oxides prepared by solution combustion synthesis as catalysts for the total oxidation of VOCs, *Appl. Catal. B: Environ.* 163 (2015) 277–287.
- [9] S. Waglechner, M. Nitzer-Noski, S. Kureti, Oxidation of soot on manganese oxide catalysts, *Chem. Eng. J.* 259 (2015) 492–504.
- [10] N.D. Wasalathantri, T.M. Santamaría, D.A. Kriz, S.L. Dissanayake, C.H. Kuo, S. Biswas, S.L. Suib, Mesoporous manganese oxides for NO<sub>x</sub> assisted catalytic soot oxidation, *Appl. Catal. B: Environ.* 201 (2017) 543–551.
- [11] Q. Fu, W.X. Li, Y.X. Yao, H.Y. Liu, H.Y. Su, D. Ma, X.K. Gu, L.M. Chen, Z. Wang, H. Zhang, B. Wang, X.H. Bao, Interface-confined ferrous centers for catalytic oxidation, *Science* 328 (2010) 1141–1144.
- [12] L. Kong, W. Wei, Q. Zhao, J.Q. Wang, Y. Wan, Active coordinatively unsaturated manganese monoxide-containing mesoporous carbon catalyst in wet peroxide oxidation, *ACS Catal.* 2 (2012) 2577–2586.
- [13] C. Tai, J.F. Peng, J.F. Liu, G.B. Jiang, H. Zou, Determination of hydroxyl radicals in advanced oxidation processes with dimethyl sulfoxide trapping and liquid chromatography, *Anal. Chim. Acta* 527 (2004) 73–80.
- [14] B.H.J. Bielski, G.G. Shiue, S. Bajuk, Reduction of nitro blue tetrazolium by CO<sub>2</sub><sup>-</sup> and O<sub>2</sub><sup>-</sup> radicals, *J. Phys. Chem.* 84 (1980) 830–833.
- [15] X. Zhu, M. Tong, S. Shi, H. Zhao, J. Ni, Essential explanation of the strong mineralization performance of boron-doped diamond electrodes, *Environ. Sci. Technol.* 13 (2008) 4914–4920.
- [16] W. Zhang, J. Sheng, J. Zhang, T. He, L. Hu, R. Wang, L. Mai, S. Mu, Hierarchical three-dimensional MnO nanorods/carbon anodes for ultralong-life lithium-ion batteries, *J. Mater. Chem. A* 4 (2016) 16936–16945.
- [17] H. Jalife-Jacobo, R. Feria-Reyes, O. Serrano-Torres, S. Gutiérrez-Granados, J.M. Peralta-Hernández, Diazoy Congo Red degradation using a Boron-doped diamond anode: an experimental study on the effect of supporting electrolytes, *J. Hazard. Mater.* 319 (2016) 78–83.
- [18] M. Murugananthan, S. Yoshihara, T. Rakumab, T. Shirakashi, Mineralization of bisphenol A (BPA) by anodic oxidation with boron-doped diamond (BDD) electrode, *J. Hazard. Mater.* 154 (2008) 213–220.
- [19] Y.H. Cui, Y.J. Feng, X.Y. Li, Kinetics and efficiency analysis of electrochemical oxidation of phenol: influence of anode materials and operational conditions, *Chem. Eng. Technol.* 34 (2011) 265–272.
- [20] R.J. Lan, J.T. Li, B.H. Chen, Ultrasonic degradation of fuchsin basic in aqueous solution: effects of operating parameters and additives, *Int. J. Photoenergy* 2013 (2013) 1–7.
- [21] Y. Wang, J. Wang, B. Du, Y. Wang, Y. Xiong, Y. Yang, X. Zhang, Synthesis of hierarchically porous perovskite-carbon aerogel composite catalysts for the rapid degradation of fuchsin basic under microwave irradiation and an insight into probable catalytic mechanism, *Appl. Surf. Sci.* 439 (2018) 475–487.
- [22] Y. Wu, S. Liu, Y. Zuo, J. Li, J. Wang, Photodegradation of some dyes over Ce/FSM-16 catalyst under solar light, *Catal. Lett.* 119 (2007) 245–251.
- [23] P. Liu, S. He, H. Wei, J. Wang, C. Sun, Characterization of α-Fe<sub>2</sub>O<sub>3</sub>/γ-Al<sub>2</sub>O<sub>3</sub> catalysts for catalytic wet peroxide oxidation of m-cresol, *Ind. Eng. Chem. Res.* 54 (2015) 130–136.
- [24] S.P.M. Menachery, T.P. Nguyen, P. Gopinathan, U.K. Aravind, C.T. Aravindakumar, Exploring the mechanism of diphenylmethanol oxidation: a combined experimental and theoretical approach, *Chem. Phys.* 513 (2018) 201–208.
- [25] G. Jing, M. Luan, T. Chen, Progress of catalytic wet air oxidation technology, *Arab. J. Chem.* 9 (2016) S1208–1213.
- [26] X. Duan, F. Ma, Z. Yuan, L. Chang, X. Jin, Electrochemical degradation of phenol in aqueous solution using PbO<sub>2</sub> anode, *J. Taiwan Inst. Chem. E.* 44 (2013) 95–102.
- [27] S. Nijjer, J. Thonstad, G.M. Haarberg, Oxidation of manganese (II) and reduction of manganese dioxide in sulphuric acid, *Electrochim. Acta* 46 (2000) 395–399.
- [28] J. Zhang, Y. Li, L. Wang, C. Zhang, H. He, Catalytic oxidation of formaldehyde over manganese oxides with different crystal structures, *Catal. Sci. Technol.* 5 (2015) 2305–2313.
- [29] L. Mao, Z. Chen, X. Wu, X. Tang, S. Yao, X. Zhang, B. Jiang, J. Han, Z. Wu, H. Lu, T. Nozaki, Plasma-catalyst hybrid reactor with CeO<sub>2</sub>/γ-Al<sub>2</sub>O<sub>3</sub> for benzene decomposition with synergistic effect and nano particle by-product reduction, *J. Hazard. Mater.* 347 (2018) 150–159.
- [30] A. Bielanski, J. Haber, Oxygen in catalysis on transition metal oxides, *Catal. Rev. Sci. Eng.* 19 (1979) 1–41.
- [31] A. Heponiemi, S. Azalim, T. Hu, U. Lassi, Cerium oxide based catalysts for wet air oxidation of bisphenol A, *Top. Catal.* 58 (2015) 1043–1052.
- [32] Y.F. Han, F. Chen, Z. Zhong, K. Ramesh, L. Chen, E. Widjaja, Controlled synthesis, characterization, and catalytic properties of Mn<sub>2</sub>O<sub>3</sub> and Mn<sub>3</sub>O<sub>4</sub> nanoparticles supported on mesoporous silica SBA-15, *J. Phys. Chem. B* 110 (2006) 24450–24456.
- [33] C.H. Kuo, I.M. Mosa, A.S. Poyraz, S. Biswas, A.M. El-Sawy, W. Song, Z. Luo, S.Y. Chen, J.F. Rusling, J. He, S.L. Suib, Robust mesoporous manganese oxide catalysts for water oxidation, *ACS Catal.* 5 (2015) 1693–1699.
- [34] M. Panizza, G. Cerisola, Direct and mediated anodic oxidation of organic pollutants, *Chem. Rev.* 109 (2009) 6541–6569.
- [35] J. Luo, Q. Zhang, J. Garcia-Martinez, S.L. Suib, Adsorptive and acidic properties, reversible lattice oxygen evolution, and catalytic mechanism of cryptomelane-type manganese oxides as oxidation catalysts, *J. Am. Chem. Soc.* 130 (2008) 3198–3207.
- [36] K.H. Kim, S.K. Ihm, Heterogeneous catalytic wet air oxidation of refractory organic pollutants in industrial wastewaters: a review, *J. Hazard. Mater.* 186 (2011) 16–34.
- [37] H. Huang, Y. Xu, Q. Feng, D.Y.C. Leung, Low temperature catalytic oxidation of volatile organic compounds: a review, *Catal. Sci. Technol.* 5 (2015) 2649–2669.
- [38] F.C. Moreira, R.A.R. Boaventura, E. Brillas, V.J.P. Vilar, Electrochemical advanced oxidation processes: a review on their application to synthetic and real wastewaters, *Appl. Catal. B: Environ.* 202 (2017) 217–261.